Dispersal of High-Burnup Fuel Fragment Surrogate Particles during and after Loss-of-Coolant Accident Tests

Peter Doyle[1*], Mackenzie Ridley[2], Jason Harp[1], Yong Yan[1], Matthew White[1], Nathan Capps[1]

[1]Nuclear Energy and Fuel Cycle Division, Oak Ridge National Laboratory, 1 Bethel Valley Road Oak Ridge, TN 37830, USA

[2]Materials Science and Technology Division, Oak Ridge National Laboratory, 1 Bethel Valley Road Oak Ridge, TN 37830, USA

[*]corresponding author: doylepj@ornl.gov

Abstract

The issue of fuel fragmentation, relocation, and dispersal is critical in the licensing and use of high-burnup (>62 GWd/MTU) nuclear fuel in light water reactors (LWRs). In this work, two test series are reported that examine the fragment dispersal during a burst event and an additional dispersal following the burst due to vibrations in the rod, such as those induced by accident recovery systems. To examine dispersal during the balloon and burst portion of a Loss-of-Coolant Accident event, HfO_2 fragments and yttria-stabilized zirconia pellets were filled into an as-fabricated cladding tube, which was then pressurized and subjected to loss-of-coolant accident testing in steam. Results from this test were found to be highly non-prototypic, and dispersal was both significantly more violent and significantly greater in magnitude than identified for actual fuel tests. These findings were attributed to the conservative (more dispersive) nature of the particles chosen for dispersal and to the details of the test conditions used that led to particularly wide bursts. The second set of tests examined dispersal following the burst when vibrations were induced in the rod, primarily via recovery activities such as Emergency Core Cooling System actuation leading to rapid water addition. Post-burst dispersal testing was performed by inducing sinusoidal oscillations with 2–25 nm peak-to-peak amplitude and 2–5 Hz frequencies in pre-burst rods that had been refilled with HfO_2 fragments or high-burnup fragment surrogate mixture of HfO_2 fragments and yttria-stabilized zirconia sands. Testing revealed that rods with large burst openings (7 mm wide in this work) led to unmitigated dispersal from above the burst zone but that smaller bursts (5 mm wide), although still much larger than the mean fragment size of 3 mm, led to effectively no dispersal because of interparticle locking. Additionally, mixture and moisture were found to impact the amount of dispersal: mixtures increased dispersal, and moisture drastically reduced it. The implications of these findings on likely dispersal from actual fuel are discussed.

Keywords: FFRD, LOCA, high burnup, dispersal, surrogate fuel

1. Introduction

During a loss-of-coolant accident (LOCA), high-burnup fuel, defined as fuel operated above 62 MWd/MTU will undergo fine fragmentation, followed by relocation and potential dispersal through the

Ridley: ridleymj@ornl.gov; Harp: harpjm@ornl.gov; Yan: yany@ornl.gov; White: whitesm@ornl.gov; Capps: cappsna@ornl.gov

Notice: This manuscript has been authored by UT-Battelle LLC under contract DE-AC05-00OR22725 with the US Department of Energy (DOE). The US government retains and the publisher, by accepting the article for publication, acknowledges that the US government retains a nonexclusive, paid-up, irrevocable, worldwide license to publish or reproduce the published form of this manuscript, or allow others to do so, for US government purposes. DOE will provide public access to these results of federally sponsored research in accordance with the DOE Public Access Plan (http://energy.gov/downloads/doe-public-access-plan).

burst opening. This process is collectively called fuel fragmentation, relocation, and dispersal (FFRD). As burnup increases, the microstructure is believed to change substantially, impacting the extent of overall and radially distributed fragmentation (Capps et al., 2021; Gerczak et al., 2018; McKinney et al., 2023; Seibert et al., 2022; Turnbull et al., 2015). Near the periphery of the fuel, the high-burnup structure is expected to lead to powder-sized fragments that are less than 1 mm in diameter. The rest of the fuel breaks into fragments, whose sizes depend on the region of the fuel from which they originate. The number and width of the microstructurally distinct fuel regions depend on the actual fuel burnup and fuel thermal history (Gerczak et al., 2018; McKinney et al., 2023; Seibert et al., 2022).

Immediately after fracture, pellet fragments are still largely bound in place by the cladding until sufficient strain is induced followed by the balloon and cladding rupture. Dispersal of fuel fragments becomes possible and the center of the burst provides a void into which the fuel fragments may fall (Flanagan et al., 2013; Raynaud, 2012; Sonnenburg, 2016). The fragments may relocate toward the burst region. Initial relocation is likely caused by the pressure wave created when the rod depressurizes following the burst. LOCA-related forces on the fuel rod (primarily flow-induced vibrations) are then responsible for additional relocation into the burst region. While relocating, the fragments have the opportunity to change orientation and potentially lock together either in the tube cross section or at the burst opening. This behavior potentially limits dispersal; however, this behavior is dependent on the size of the burst. Capps et al. identified a threshold approximate burst area of 80–100 mm^2, above which significant dispersal is expected and below which dispersal is expected to be minimal (Capps et al., 2021). The blowdown-induced dispersal effect was investigated with surrogate particles by researchers at Oregon State University (Campos et al., 2023; Latimer et al., 2020). In those publications, the researchers found a substantial impact of opening geometry, particle size, and blowdown pressure on final burst and importantly found particle locking effects in the burst opening when the particle-to-burst size ratio was at or under 2.

This work examined dispersal (1) during the initial burst of a surrogate rod with surrogate particles and (2) following burst and during recovery operations that induce vibrations into the rods. Effects of fill particles and LOCA conditions on burst-induced dispersal and effects of fill particles, moisture, burst geometry, and induced vibration parameters on post-burst dispersal were examined.

2. Experimental Design

The present work consisted of two parts to simulate fuel dispersal. First, the Severe Accident Test Station (SATS) at Oak Ridge National Laboratory (ORNL) was used to simulate burst of high-burnup fuel rods and the dispersal occurring during the burst event. SATS consists of two modules: one furnace for integral testing LOCA scenarios and the other furnace with a high-temperature furnace for testing fuel segments in beyond design basis accidents (Snead et al., 2015; Yan et al., 2017). The tests in this work were conducted in the LOCA furnace. The test temperature was monitored and recorded with a Type-S thermocouple in the furnace. Second, rods previously burst in LOCA SATS tests were filled with surrogate fuel particles, the rods were then loaded into the Fuel Relocation Induced by Accident Recovery (FRIAR) system and subjected to vibrations, and dispersed mass was measured.

2.1 Surrogate High-Burnup Fuel Simulant Particles

Three types of high-burnup surrogate materials were used in this test. The first was HfO_2 pellets and were chosen for their density and fragment-like appearance. These particles had an average size of 3 ± 1

mm and were purchased from MSE Supplies (model TA2253). Yttria-stabilized zirconia (YSZ) spheres of various sizes were purchased from Micro Milling Media. Beyond the lower density, these also do not pack and have less interparticle friction as the fragment-like HfO_2 particles and thus represent the most conservative condition for dispersal because of minimal packing-induced dispersal restraint. Additionally, the YSZ particles were very precise in size and were procured in three diameter spheres: 0.3–0.4, 0.9–1.1, and 3 mm corresponding to model numbers BA0101, BA0118, and BA0109, respectively. A third surrogate material was created by mixing the YSZ particles of various sizes and the large HfO_2 fragments. This surrogate material is referred to as the *mixture* filler throughout this work.

Although actual high-burnup fuel undergoes fragmentation differently depending on fuel thermal history and actual burnup, the observed post-test fragment distribution is roughly similar across various conditions (Capps et al., 2020; Sonnenburg, 2016). The NA#2 test fragment distribution reported by Capps et al. (Capps et al., 2020) was used as the basis of the *mixture* filler. This mix contained 60 wt % HfO_2, 25 wt % 0.9–1.1 mm YSZ, and 15 wt % 0.3– 0.4 mm YSZ which is volumetrically similar to the particles that were sieved from the NA#2 test. An additional 5 g water/g mixture was added to this mixture to create a *wet mixture* for a select test condition. This amount of water caused weak adhesion of small and large particles, similar to observations of *sticky* fuel in LOCA tests on actual fuel. Figure 1 shows images of (a) the HfO_2 particles, (b) the 3 mm YSZ particles, and (c) the wet mixture.

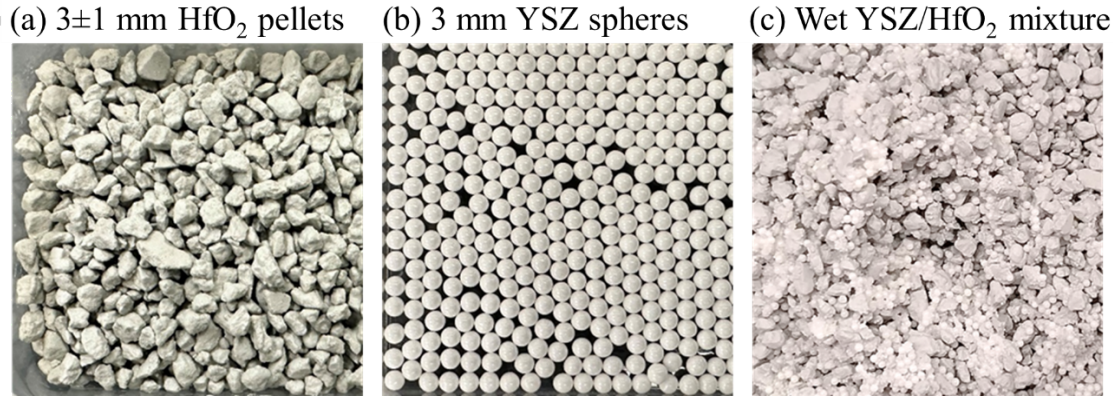

Figure 1. Surrogate high-burnup fuel simulant materials. Variously shaped HfO_2 fragments (a) with an average size of 3 ± 1 mm, (b) 3 mm diameter YSZ spheres, and (c) wetted mixture simulant.

2.2 LOCA Simulant Tests with Simulated High-Burnup Fuel Fragments

Dispersal tests were accomplished in the ORNL SATS for non-radiological materials (Bell et al., 2021; Capps et al., 2020; Kane et al., 2021). Stressed-relieved and annealed Zircaloy-4 rods were procured from Cameco Fuel Manufacturing. See Table 1 for a summary of material properties. These rods were assembled into the SATS test train using Swagelok fittings after being filled with the relevant surrogate particles. They were then pressurized to approximately 8.5 MPa at room temperature and then sealed off from the gas supply such that pressure would vary throughout the test as tube temperature and integrity changed. The rods were heated at either 1 or 5 °C/s using a 4-lamp, 8 kW infrared furnace with a 100% steam flow. Throughout the tests, sample temperature was monitored by type-S thermocouples at the same axial location and on opposite sides of the tube. One of these thermocouples was used to control the temperature of the test, and the other was used as a safety limit.

Table 1. Dimensions and nominal chemical composition of Zircaloy-4, ASTM B353 (ASTM, 2022).

Parameter	Zircaloy-4
Length (mm)	304.8
Width (mm)	9.50
Thickness (mm)	0.56
Zr (wt %)	Balance
Sn (wt %)	1.20–1.45
Fe + Cr (wt %)	0.37
Cr (wt %)	0.07–0.13
Ni (wt %)	—

In each test, the sample was heated to 100°C, and steam was injected into the furnace. Once steam flow had equilibrated, the furnace was ramped to 300°C and held for 5 min to simulate normal power operations. Following the hold, the specimen was heated at either 1°C/s or 5°C/s until the cladding ruptured, at which point power was shut off, and the sample was allowed to cool to ambient conditions. During these tests, stainless-steel shields were introduced around the central SATS quartz tube to protect operators during testing.

Three SATS tests were conducted for this work. The first was a baseline SATS test with an intact Al_2O_3 rod to simulate a non-dispersal test. A second test was run with only 3 mm YSZ pellets, followed by a final test with only the HfO_2 fragments. The first two tests were ramped at 5°C/s, and the final test with the HfO_2 fragments was run with a 1°C/s ramp rate. The lower ramp rate of the last test was run to assess the potential impact of the lower ramp rate and increased interparticle packing interactions on dispersal behavior. Following testing under each condition, the rod was examined with a Keyence VR-3100 digital macroscope to evaluate the burst opening, and any dispersed material was also collected and weighed.

2.3 Design of the FRIAR Apparatus and Testing Procedure

FRIAR was designed to induce specific vibrations in a SATS sample train, collect the dispersed material, and record the mass of material collected. As shown in Figure 2, FRIAR consists of a sample tray which mates to a SATS test train. Test oscillations were then induced by an Ultra Motion A2PZ8A servo motor, causing the sample tray to glide over supporting bearing plates. Underneath the bearing plates, a guide tube ran down to the collection tray, which was positioned on an Ohaus PA1502 mass balance with a resolution of 0.01 g. The servo motor was configured to move based on a voltage signal, which was provided by a B&K waveform generator (4055B). This setup is shown in Figure 2.

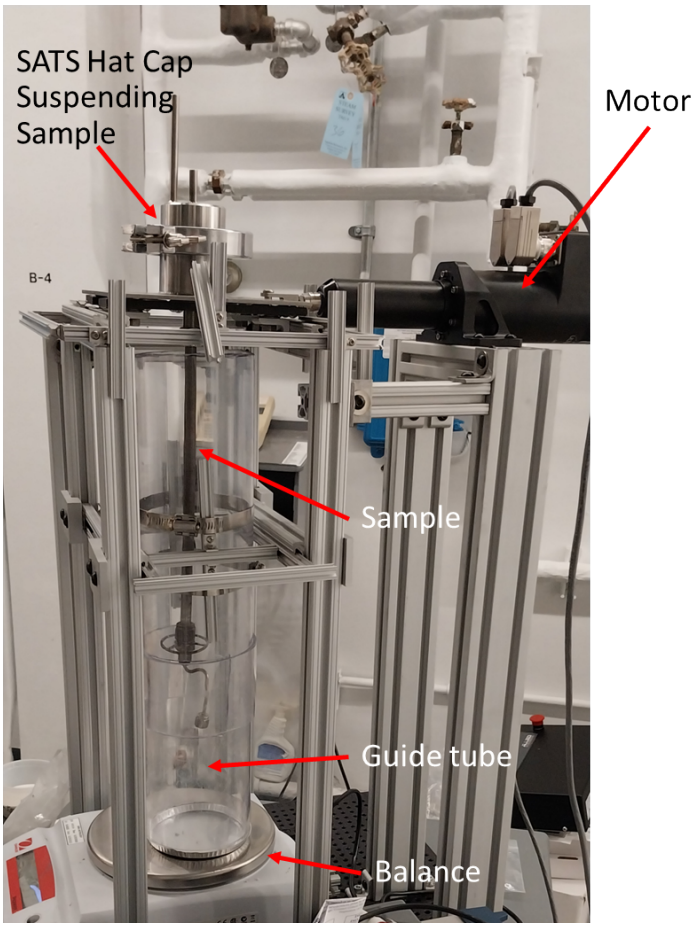

Figure 2. FRIAR apparatus and the system components.

During deployment, a voltage-to-distance factor was determined via a multistep calibration in which the factor was determined for an oscillation at 2 Hz and 25 mm amplitude. The target amplitude was then decreased in several steps down to 0.5 mm and the error assessed to be less than 1%. Following that step, a capability assessment was performed by varying the frequency and amplitude and observing the actual displacement waveform of the motor. To a rough approximation, the sinusoidal motion of the system was limited by $F = 14.8 - 3.91 \ln(A)$, where *F* is the maximum frequency in hertz and *A* is the peak-to-peak amplitude in millimeters. Amplitudes were generally limited to $0.5 \leq A \leq 25$ mm, and *F* was limited accordingly. At any given amplitude, frequencies as low as 0.5 Hz were tested and all successfully produced the required position waveform.

For actual operation, a LabVIEW Virtual Instrument control code was written to control the waveform generator and record mass data from the mass balance and position data from the servo motor throughout the test. Position data from the servo motor examined during each test; the servo motor maintained precision and accuracy across the test campaign. Each test used a pre-burst rod that had been emptied of any components remaining from the corresponding SATS test. The rod was then filled with the particle type of interest and swaged to the SATS hat cap and weighed. This method of preloading was preferred to a direct test after a surrogate SATS test, such as reported in section 3.1, because of the non-prototypic nature of the dispersal observed in those tests. The loaded rod was secured to the mobile frame, and the mass of any material that fell out of the rod during loading was

recorded. This mass lost during loading was generally limited to a few small particles in the mouth of the burst. After the 5 min test, the amount lost during the test was recorded (the full stream of balance values was also recorded throughout the test). The rod was then unloaded from the system.

2.4 FRIAR Simulant Tests

FRIAR tests described herein were divided into investigations of the following features: (1) particle type, (2) burst geometry, and (3) vibration frequency and amplitude. Because this work is preliminary, the authors have not attempted to fully explore the expected analysis space.

For initial tests, the capability of a rod to retain the largest fragments was explored. All tests in this batch were conducted with dry particles, and each condition was tested five times to generate statistics. Two burst geometries were selected. The first was a 7 mm wide and 15.5 mm long ovular burst. The overall burst area was initially selected as much larger than the average particle size of HfO_2 (3mm) and yet small enough that some locking of the particles in the burst could occur. Initial testing explored low-frequency (2 Hz) vibrations with amplitudes from 2 to 25 mm. Based on the results of that test, higher-frequency (5 Hz) vibrations at low (2 mm) amplitude were also conducted.

This first round of tests led to a subsequent choice of a smaller burst geometry: 5 mm wide and 13.5 mm long. Although a significantly smaller burst width, this width was still more than 1.5 σ above the mean particle size, and the vast majority of particles were plainly able to disperse through the opening absent particle locking effects. Additionally, the burst was more rectangular than the rod with a larger burst opening. With the smaller-burst sample rod, the same 5 Hz test was repeated at 2 and 5 mm amplitudes, and a follow-up test was conducted at 2 Hz and 25 mm.

The results of these tests led to the choice of the 5 mm wide and 13.5 mm long burst tube for subsequent mixture dispersal analysis, which was conducted in limited tests at 5 Hz and 2 or 10 mm. For the mixture tests, the variable nature of the mixture led to packing differences among the loadings, and care was taken to ensure the mixture was as homogeneously dispersed into the tube as possible. For the wet tests, only three tests were performed within a day. After three consecutive tests, scatter among the results increased. After the three tests, the rod was fully emptied, and both the particles and the rod were dried in air overnight, followed by rewetting of particles and retesting of the rod. On retest, the data were consistent with initial tests from the previous day. Thus, all wet testing was determined to be representative for up to three consecutive tests. A summary of the test matrix in this work is provided in Table 2.

Table 2. Test matrix of FRIAR dispersal tests.

Fill Material	Burst Geometry	Frequency (Hz)	Peak-to-peak amplitude (mm)
HfO_2 fragments	7 mm wide 15.5 mm long	2	25
		2	10
		2	5
		2	2
		5	2
	5 mm wide 13.5 mm long	5	10
		5	2
		2	25
Mixture	5 mm wide	5	10

	13.5 mm long	5	2
Wet mixture		5	10

3. Results

3.1 LOCA Simulant Tests with Simulated High-Burnup Fuel Fragments

Temperature and pressure plots from all three in-burst dispersal simulant tests are shown in Figure 3. The temperature axes were the same across all three plots, and the pressure axes uniformly showed a pressure range of 2.5 MPa. The control and limit thermocouples (which were in the same axial position but on opposite sides of the rod) for all tests followed the same trajectory and were only several degrees centigrade apart, indicating approximately uniform azimuthal heating. Moreover, during heating, the internal rod pressure followed rod temperature until the rod entered the ballooning and burst phase. This behavior was expected due to gas expansion during heating.

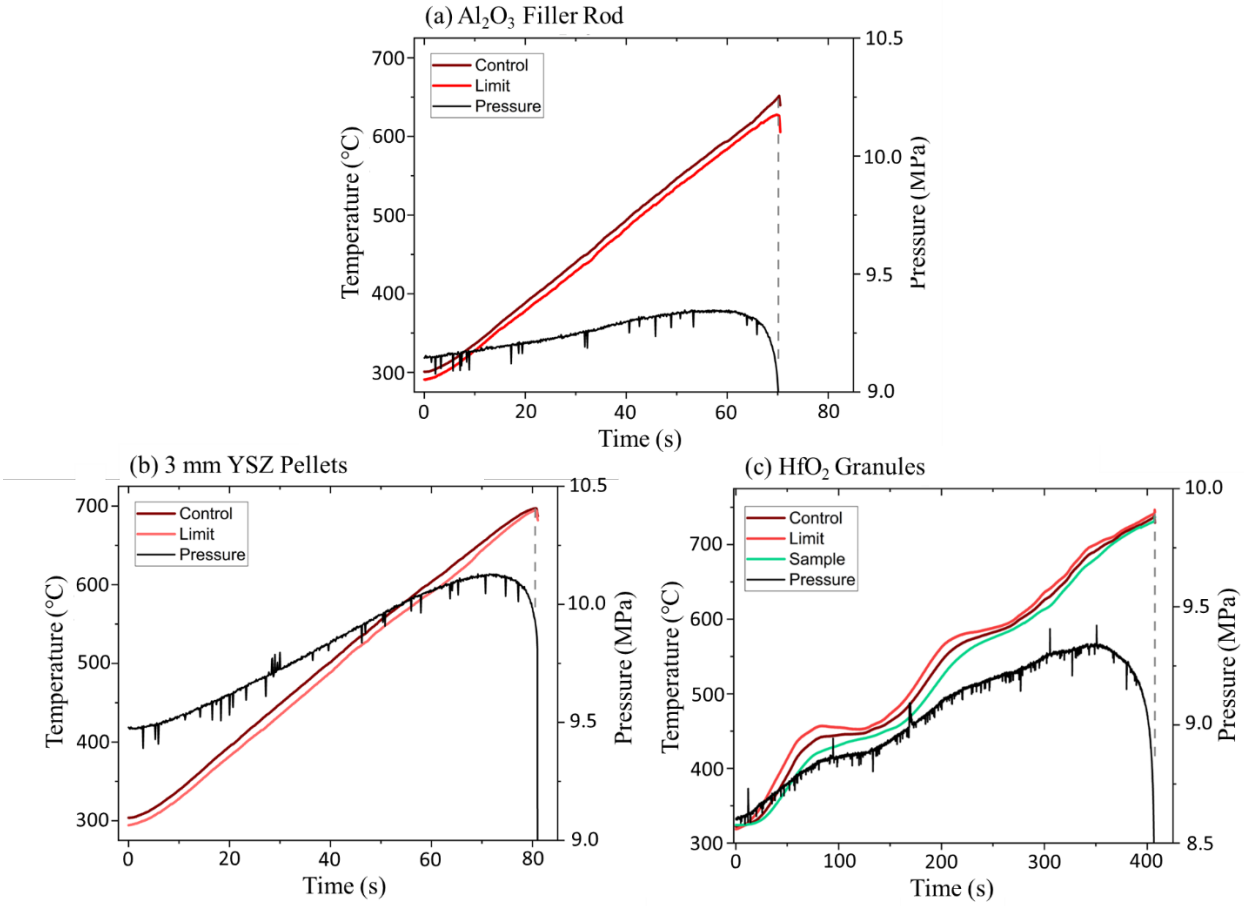

Figure 3. Temperature and pressure history during SATS-simulant dispersal tests in (a) baseline conditions with the A_2O_3 filler rod, (b) 3 mm YSZ particles, and (c) HfO_2 fragments.

In the first test, Figure 3(a), the heating rate was entirely linear. The onset of ballooning, as evidenced by the pressure curve plateau, occurred at 580°C, and a cladding rupture occurred at 650°C. Throughout

the test, the pressure increased by approximately 0.2 MPa. Because no dispersible materials were used in the first test (only solid Al_2O_3 filler rods), no dispersal was observed.

The second test, Figure 3(b), also exhibited linear heating with a ballooning onset at approximately 650°C and burst at 690°C. Unlike in the first test, the tube pressure increased significantly more: by 0.6 MPa compared to that of the beginning of the test. In this test, the YSZ particles were partially dispersed, and only 59% was retained. Furthermore, the dispersal came mostly from particles below the burst, whereas particles above the burst remained packed above the burst in the tube.

Finally, the HfO_2 test, Figure 3(c), exhibited somewhat different characteristics than those of the other tests. Whereas the other tests showed linear heating, the comparatively low heating rate of 1°C/s led to difficulty in the furnace heating at the desired rate, especially at a lower temperature. However, the average heating rate was approximately 1°C/s. Correspondingly, the pressure curve was slightly nonlinear with time as the tube pressure followed the actual tube temperature. Ballooning in the HfO_2 test began at approximately 700°C, and the final burst occurred at 740°C. During the test, an absolute pressure change of approximately 0.75 MPa occurred. Dispersal in this last test was nearly complete, and only a few grams of the initial 52 g of fragments were left after the test. In both dispersal tests, the dispersing material was ejected at great force, destroying the enclosing SiO_2 tube and causing damage to the surrounding lamps.

Images of rods after each test are provided in Figure 4 after analysis with the Keyence macroscope. In the first test, Figure 4(a), the burst exhibited an hourglass appearance and was quite small. At its maximum width, the burst was only 1.9 mm wide, and the burst was 9.5 mm long. Both subsequent tests significantly differed in both shape and size. The 3 mm YSZ particle test, Figure 4(b), was most like an oval, but it could also be described as rectangular. The burst length was 11.1 mm, and the burst width was 7.0 mm. The HfO_2 test was larger still, Figure 4(c), with a 21.2 mm long burst and associated 12.0 mm width. This shape also fits the semi-oval, semi-rectangular shape category. Detailed burst parameters for the three tests are presented in Table 3.

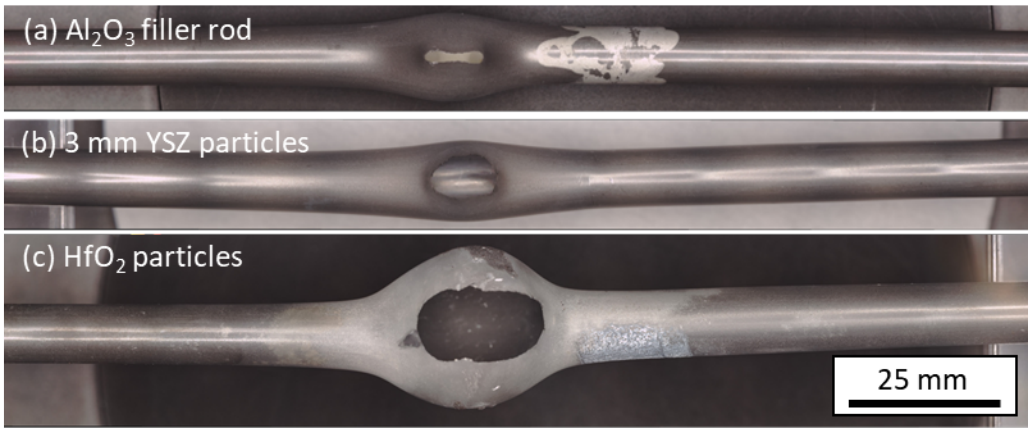

Figure 4. Test rods from each condition following exposure in (a) baseline conditions with the A_2O_3 filler rod, (b) 3 mm YSZ particles, and (c) HfO_2 fragments.

Table 3. Burst parameters and select test conditions from LOCA simulant SATS dispersal testing using various fill materials.

Parameter	Al_2O_3 rod baseline	3 mm YSZ pellets	HfO_2 granules
Heat rate (°C/s)	5.1	5.2	1
Rupture temperature (°C)	650	690	740
Maximum diametric strain (%)	51	56	162
Burst opening area (mm^2)	15	63	200
Maximum width of burst (mm)	1.9	7.0	12.0
Length of burst (mm)	9.5	11.1	21.2

3.2 FRIAR Dispersal Results

All dispersal tests in this work were run for 5 min. However, in all tests, most dispersal occurred within the first 60 s of the test. For the 2 Hz frequency tests, the dispersal took slightly longer, but in no case did the tube continue to disperse material within the last 60 s of the test. Results from the tests were classified based on the burst geometry used to produce the burst. Figure 5 and Figure 6 show the cumulative mass loss throughout each test using the rod with a larger burst (7 mm wide) and the rod with a smaller burst (5 mm wide), respectively. In both curves, the test conditions are printed along the x-axis showing particle type, sinusoidal frequency, and peak-to-peak wave amplitude. Mass loss magnitudes are given in grams, and the standard deviation of the mass loss across all tests in the set is shown as error bars. In a few cases, the standard deviation in a plot extends to negative numbers because the tests in each condition did not always fit a Gaussian distribution, and the scatter among tests for those conditions was high. Definitions of mixture and wet mixture are provided in the legend and in section 2.1.

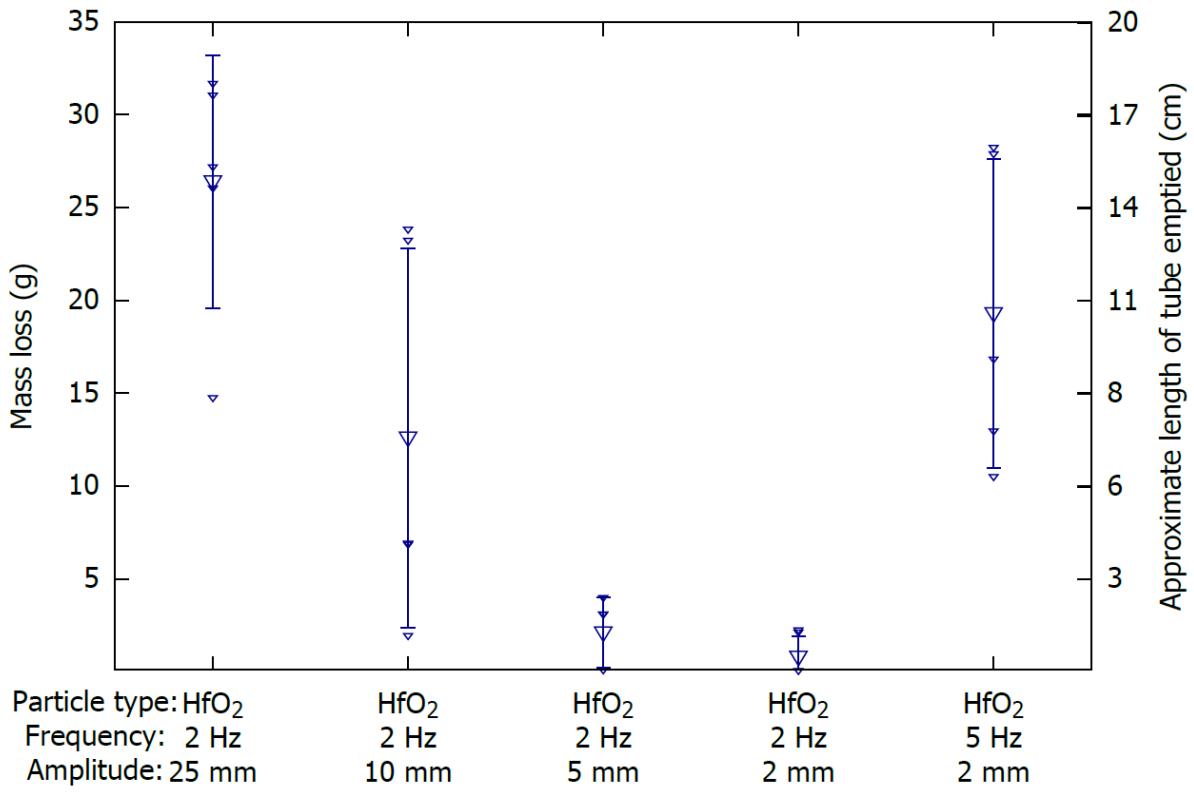

Figure 5. Dispersed mass during FRIAR tests involving a rod with a 7 × 16 mm oval burst. The equivalent length of the tube which has been emptied due to given mass lost is given on the secondary y-axis. Each test condition was performed with the HfO_2 fragments. All tests were performed with sinusoidal oscillations with frequency and peak-to-peak amplitude for each test given along the x-axis. Large, inverted triangles correspond to the average values, and smaller inverted triangles show individually gathered data points.

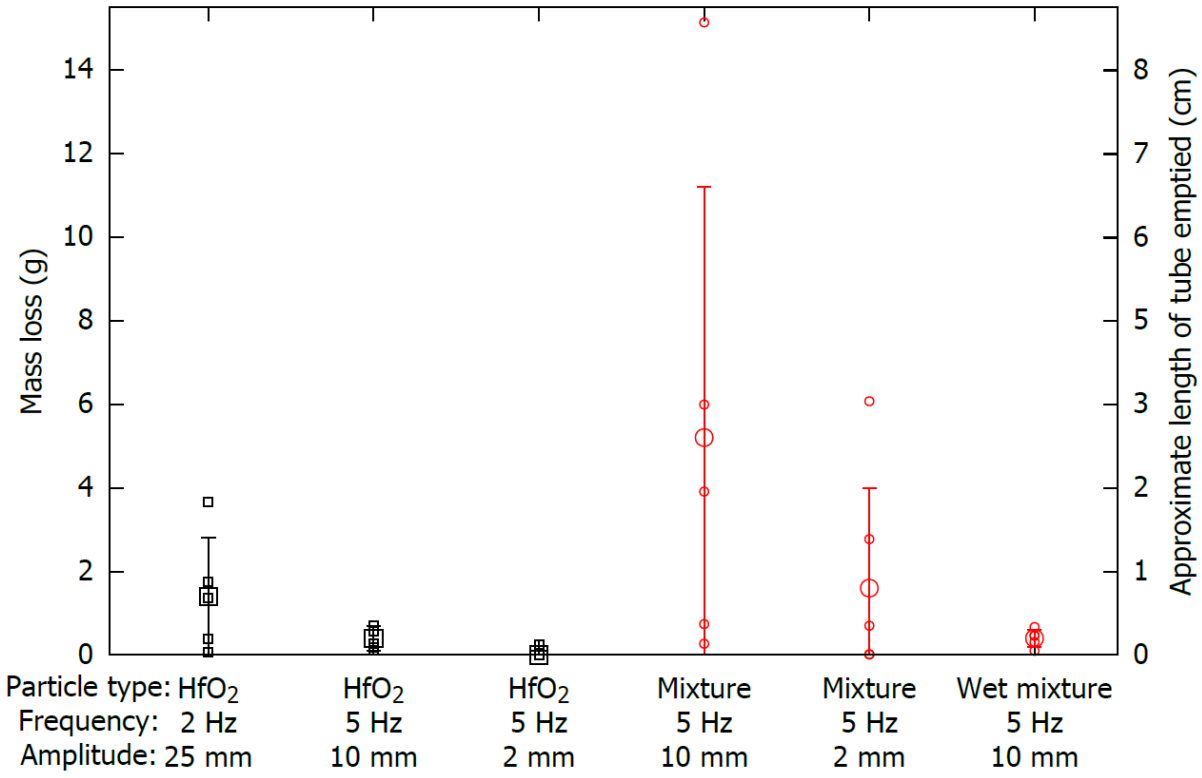

Figure 6. Dispersed mass during FRIAR tests involving a rod with a 5 × 14 mm rectangular burst. The equivalent length of the tube which has been emptied due to given mass lost is given on the secondary y-axis. Black squares show tests with only HfO_2 fragment parts. Red circles show tests with mixtures containing 60 wt % HfO_2 fragments, 25 wt % 0.9–1.1 mm YSZ spheres, and 15 wt % 0.3 – 0.4 mm YSZ spheres—similar to the fragment sizes for the NA#2 test reported by Capps et al. (Capps et al., 2020), Table 5 of that work). All tests were performed with sinusoidal oscillations with frequency and peak-to-peak amplitude for each test given along the x-axis. Large squares and circles indicate averages of the dataset, and small squares and circles indicate individually collected data points.

In Figure 5, the first four datasets represent dispersal at 2 Hz and amplitudes of 25, 10, and 2 mm. All three of these test conditions demonstrated a lack of any restraint against particle dispersal. Particles were dispersed freely from the burst in the 25 mm case and always resulted in complete loss of particles from the space above the burst region. The scatter in data points represents only the difference in initial particle loading above the burst region. Naturally, as the impulse to the particles decreased to 10 mm and then 2 mm, the energy delivered to the particles decreased, and fewer of them dispersed from the burst. At 2 mm, effectively no dispersal outside the primary burst region was observed. However, by increasing the frequency to 5 Hz, dispersal significantly increased to near complete loss of loading material.

At the lower burst width of 5 mm, Figure 6 shows that none of the examined conditions caused full loss of loading above the burst. The most aggressive conditions employed, 25 mm at 2 Hz and 10 mm at 5 Hz, resulted in only a few grams of loss per test and very little scatter. Visual examination of the rods during oscillation found no sign of actual particle motion except for a few scattered particles falling out

of the front of the burst region in the first few seconds of the test. This behavior changed slightly when the HfO_2 particles were substituted for the high-burnup surrogate mixture.

For that mixture at the most aggressive 10 mm at 5 Hz condition, the scatter increased dramatically with very little dispersal in some tests and significant dispersal of several grams in other tests. One of the individual tests, as shown by the red circles, resulted in just over 15 g of dispersed material: nearly half of the original loading. Similarly, the lower-amplitude 2 mm at 5 Hz condition resulted in large dispersal scatter but a smaller average mass loss. The maximum test loss was also approximately half of the 10 mm case at just over 6 g. Wetting the mixture and subjecting the rod to the aggressive 10 mm oscillation at 5 Hz reduced the magnitude and scatter in the data compared to the dry mixture. All tests dispersed less than 1 g of material, and nearly no variation occurred between tests.

4. Discussion

4.1 Assessment of the Present Particle Groups as Surrogates for Nuclear Fuel Fragments

The three LOCA-type tests were used in this work primarily to show the degree of surrogacy of the present particles compared to actual fuel. During burst, the fused Al_2O_3 rods led to a small burst at the lowest temperature. In comparison, the same conditions with YSZ particles led to a larger burst at a higher temperature. The increased burst temperature when using YSZ particles was likely caused by differences in contact of the rod with the cladding compared to the particles with the cladding. The fused rod was not in complete contact with the cladding, allowing a hot spot on the cladding to lead to failure quickly and at a lower recorded temperature. In contrast, the YSZ particles were packed together and in contact with the cladding. Thus, as the burst region developed, the local heating could spread over a larger area, thus allowing the burst region as measured by the thermocouple to reach a slightly higher temperature and pressure before burst. The fused Al_2O_3 rod test performed in this work was atypical of such tests. Normally tubes filled with Al_2O_3 rods burst at temperatures and pressures near 730 °C and 9.6 MPa, respectively, which are similar to where the YSZ-filled cladding burst (Capps et al., 2023; Kane et al., 2022; Ridley et al., 2023), implying ordinarily better contact between the fused rods and the cladding than in this work.

Similarly, the burst for the cladding filled with HfO_2 particles was significantly larger, both in strain and opening size, than that of the YSZ particles. The differences in particles (better thermal contact between the HfO_2 and cladding compared to YSZ and cladding) may have contributed to the differences in burst behavior. However, thermal contact is unlikely to fully explain the differences in these two tests. First, both tests would likely have had similar thermal contact. The better packing of the HfO_2 particles may have led to a marginal improvement in local thermal equalization, but contact would likely have been similar between the tests, and particles in each test were of approximately similar sizes. Second, the tests were run with significantly different heat rates (5°C/s vs. 1°C/s). At a lower heat rate, the HfO_2-filled cladding spent 5× more time in the transient regime, thereby leading to two related effects. Creep was more significant, particularly as temperature increased, causing maximal diametric strain to be 162%, far more than observed in most LOCA simulant burst conditions for real or simulant fuel (Bell et al., 2021; Flanagan et al., 2013; Kane et al., 2022; Raynaud, 2012). The significant extra volume added to the tube by this strain reduced the overall pressure in the tube at a higher temperature, further

elevating the burst temperature. At the moment of burst, the wall thickness was thus much less than in the other two tests, thereby providing less restraint and a larger burst. Both the YSZ-filled and HfO_2-filled cladding tests resulted in bursts that were substantially larger than those observed in many literature tests (Bell et al., 2021; Flanagan et al., 2013; Kane et al., 2022; Raynaud, 2012).

Besides the details of the burst mechanism, the particles failed to disperse similarly to those in any known fuel tests (Capps et al., 2021; Capps et al., 2020; Flanagan et al., 2013; Raynaud, 2012). Both dispersed violently and caused damage to the enclosing materials and furnace. Moreover, the YSZ particles dispersed from the bottom of the rod, whereas the particles above the burst were stuck together. For the HfO_2 tests, the dispersal was even more substantial, effectively fully removing the full particle loading. The level and force of dispersal of these particles greatly differed from those observed fueled tests, which have shown relocation from above the burst rather than below. For the YSZ particles, the level of dispersal is reasonable. The spherical particles provided little-to-no interparticle friction; the only particle locking was contributed by pressure packing of particles together either during the burst or throughout the test. The HfO_2 particles, as shown by the FRIAR dispersal tests in this work, by contrast did exhibit interparticle locking restraint but only for smaller burst sizes (at 5 mm wide bursts in this work). The slower ramp time in this work led to such a large burst, 12 mm wide, that no interparticle locking occurred. Thus, the particles were effectively blown out of the burst region.

Taken together, the present burst-induced dispersal tests did not successfully serve as surrogates for fragmented fuel during burst. The bursts were significantly larger, and dispersal was significantly more violent than observed in actual burst tests, indicating the need for further development of a surrogate or the need to study this on irradiated fuel.

4.2 Analysis of FRIAR Dispersal Tests

Although the particles used in this work were substantially more dispersive than actual fuel, they were still useful in the present test for representing an upper limit on material dispersed during accident conditions. The dispersal behavior in the large 7 mm wide burst tube is worth discussing. Figure 5 shows that these particles are in no way impeded from dispersing through the large 7 mm wide burst. This finding is not particularly surprising because the hole was more than 1 mm larger than all particles present in the test, and the ratio of dispersal opening to mean particle size was greater than 2 (Campos et al., 2023). Only very high interparticle friction and low vibration impulse energy could prevent dispersal under the conditions. This is reinforced by the significant increase in mass (to 18 g) when increasing the frequency to 5 Hz from 2 Hz. Additional tests are needed to examine whether dispersal would be reduced with different particle types. Campos et al. (Campos et al., 2023) similarly observed significant increases in blowdown dispersal for 1 mm HfO_2 particles compared to 2 mm particles dispersing through the same opening.

Furthermore, the same particles in the tube with the smaller 5 mm wide burst effectively did not disperse when only filled with HfO_2. At 5 mm with a semi-rectangular burst, over 90% of the HfO_2 particles were small enough to fit through the 5 mm wide opening. However, in multiple tests at each condition and when particles were not sharp or rough but smooth compared to actual fuel particles, no dispersal of note occurred. Instead, dispersal was limited to particles just at the burst opening, and the dispersal of those particles did not lead to subsequent dispersal of additional materials. Instead, they were locked in place even under a very aggressive 10 mm vibration at 5 Hz. Similar locking observed by

Campos et al. and Latimer et al. during blowdown testing of surrogate rods (Campos et al., 2023; Latimer et al., 2020).

This locking behavior is further influenced by the mixture composition and associated particle friction. During dispersal, the small particles within the mixture can become wedged between the larger particles, preventing their various faces from touching (and thereby from interacting to lock together). Additionally, this locking behavior results in more stochastic dispersal. Despite great care to maximize uniformity of the added mixture, post loading the stack was always somewhat heterogeneous in distribution. Thus, in some cases, the burst region would be populated by a locally small-particle-deficient mixture leading to more locking than the bulk, and in some cases, the burst would locally have more small particles than bulk leading to increased dispersal. Small particles are also more mobile than large ones and can migrate down the tube during the test and potentially assist in unlocking larger particles from each other. All together, these various conditions lead not only to increased dispersal overall but also to increased standard deviation due to varying true loading conditions. Additionally, because of the roundness and smoothness of the YSZ particles, it is expected that the large-particle delocking impact of the small particles in this work represents the maximum delocking effect of small particles. Small fuel fragments by contrast are unlikely to be smooth or spherical (McKinney et al., 2023; Seibert et al., 2022) and may not contribute to delocking at all. Finally, dry, smooth particle additions tend to reduce large-particle locking, increase overall dispersal, and make the tests more stochastic.

Additionally, a small amount of moisture, which is commonly present in post-burst fuels (Capps et al., 2020; Flanagan et al., 2013) creates additional particle-to-particle adhesion through surface tension and provides a highly effective particle restraining force that completely negates the impact of the small particles to reduce friction. This effect is significant enough to render the wet mixture test identical to the corresponding dry HfO_2 test for this burst size. Thus, for out-of-pile LOCA tests, if the fuel is sufficiently moistened by the steam during the burst event, then the mixture effect can be ignored, and conclusions drawn from large particles alone can sufficiently describe dispersal. Naturally, it is unknown whether the 5 wt % water added to the mixture is substantially similar to the moisture in post-burst fuel, and future work will be directed to examine the impact of additional moisture content and to evaluate its similarity to actual fueled tests. Moreover, during an actual LOCA, the fuel itself will be much hotter than during externally heated LOCA simulant tests, preventing particle wetting until the Emergency Core Cooling System quench sufficiently cools the fuel. Therefore, moisture is likely to decrease fuel dispersal post-quench, but is unlikely to play a role in mitigating dispersal between the burst event and the completion of quench. The impact of moisture on particle retention in LOCA-simulant testing of real fuel is reserved for future work.

Finally, the present tests have no bearing on the initial burst dispersal. To be representative of fuel, the fuel in the burst zone itself must be sufficiently fragmented and randomly oriented to lead to the locking effect. If the fuel at the burst location is dispersed during the burst, then the dispersal event and any subsequent relocation may sufficiently mix fuel relocating into the burst and create the observed locking effect. The present work also does not address the impact of rod pressure and blowdown effects. Additional work is needed to determine these behaviors.

5. Conclusions and Future Work

FFRD is a critical problem to understand for the licensing and use of high-burnup nuclear fuel in light-water reactors. In this work, the dispersal part of FFRD was examined with surrogate fuel particles both

during initial burst and then later because of post-burst forces on the rod, particularly as caused by the Emergency Core Cooling System and post-LOCA handling. Dispersal during burst using either YSZ particles or HfO_2 fragments as surrogates for fragmented fuel resulted in non-prototypic balloon and burst and resulted in violent and extensive expulsion of fragments leading to damage to the heating furnace. Such behavior has not been seen for actual fuel specimens, indicating that the particles used in this work result in overestimates of dispersal compared to actual conditions.

Despite the extensive dispersal during initial burst, the same overly dispersive particles were found to lock together when dispersed from a tube with a 5 mm width burst. This conclusion indicates that the minimum-dispersible width can potentially be significantly larger than that of most particles and still result in only a few grams of dispersal. However, if the fuel fragments are dry, and the small components of the fragments are sufficiently smooth, then the uncertainty may increase substantially, and the average dispersal will increase marginally. The presence of water in the post-burst fuel also appears to work against this small-particle behavior by increasing the friction between fragments. None of these effects were observed when dispersing using a tube with larger 7 mm wide burst. Additional work is underway to more extensively use the FRIAR system in examining actual high-burnup fuel following LOCA testing and further evaluating the effects of burst geometry, surrogate particle mixture composition, and vibration parameters.

Acknowledgments

The authors gratefully acknowledge the work of Adam Willoughby and Brandon Johnston in the operation of the SATS system as well as Craig Gray for assistance in the assembly of the FRIAR system. This work was funded by the US Department of Energy's Advanced Fuels Campaign. We thank Ethan Barlow for helpful technical editing work. Casey McKinney and Maxim Gussev provided helpful technical reviews.

Data Availability

Data generated in this work is available upon request.

References

ASTM, 2022. Standard Specification for Wrought Zirconium and Zirconium Alloy Seamless and Welded Tubes for Nuclear Service (Except Nuclear Fuel Cladding).

Bell, S.B., Kane, K.A., Massey, C.P., Baldesberger, L.A., Lutz, D., Pint, B.A., 2021. Strength and rupture geometry of un-irradiated C26M FeCrAl under LOCA burst testing conditions. Journal of Nuclear Materials 557, 153242.

Campos, S.D., Howard, T.K., Hendrickson, G., Weiss, A., Mignot, G., Marcum, W., 2023. Initial Characterization of Observed Dispersion and Relocation Phenomena

During a Loss of Coolant Accident (LOCA), 20th International Topical Meeting on Nuclear Reactor Thermal Hydraulics. American Nuclear Society, Washington, D.C., pp. 2182-2195.

Capps, N., Jensen, C., Cappia, F., Harp, J., Terrani, K., Woolstenhulme, N., Wachs, D., 2021. A Critical Review of High Burnup Fuel Fragmentation, Relocation, and Dispersal under Loss-Of-Coolant Accident Conditions. Journal of Nuclear Materials 546, 152750.

Capps, N., Ridley, M., Yan, Y., Bell, S., Kane, K., 2023. BISON validation to in situ cladding burst test and high-burnup LOCA experiments. Annals of Nuclear Energy 191, 109905.

Capps, N., Yan, Y., Raftery, A., Burns, Z., Smith, T., Terrani, K., Yueh, K., Bales, M., Linton, K., 2020. Integral LOCA fragmentation test on high-burnup fuel. Nuclear Engineering Design 367, 110811.
Flanagan, M.E., Askeljung, P., Puranen, A., 2013. Post-Test Examination Results from Integral, High-Burnup, Fueled LOCA Tests at Studsvik Nuclear Laboratory. US. NRC.
Gerczak, T.J., Parish, C.M., Edmondson, P.D., Baldwin, C.A., Terrani, K.A., 2018. Restructuring in high burnup UO2 studied using modern electron microscopy. Journal of Nuclear Materials 509, 245-259.
Kane, K., Bell, S., Garrison, B., Ridley, M., Gussev, M., Linton, K., Capps, N., 2022. Quantifying deformation during Zry-4 burst testing: a comparison of BISON and a combined in-situ digital image correlation and infrared thermography method. Journal of Nuclear Materials 572, 154063.
Kane, K.A., Stack, P.I.M., Mouche, P.A., Pillai, R.R., Pint, B.A., 2021. Steam oxidation of chromium corrosion barrier coatings for sic-based accident tolerant fuel cladding. Journal of Nuclear Materials 543, 152561.
Latimer, G.D., Marcum, W.R., Jones, W.F., 2020. Dispersion of Surrogate LWR Fuel Experiments Under LOCA Conditions. Nuclear Technology 206, 1374-1384.
McKinney, C., Seibert, R., Werden, J., Parish, C., Gerczak, T., Harp, J., Capps, N., 2023. Characterization of the Radial Microstructural Evolution in LWR UO2 Using Electron Backscatter Diffraction. Journal of Nuclear Materials 585, 154605.
Raynaud, P.A.C., 2012. Fuel Fragmentation, Relocation, and Dispersal During the Loss-of-Coolant Accident. U.S. NRC., NUREG-2121.
Ridley, M., Bell, S., Garrison, B., Graening, T., Capps, N., Su, Y.-F., Mouche, P., Johnston, B., Kane, K., 2023. Effects of Cr/Zircaloy-4 coating qualities for enhanced accident tolerant fuel cladding. Annals of Nuclear Energy 188, 109799.
Seibert, R.L., Werden, J.W., Parish, C.M., Harp, J.M., Gerczak, T.J., Capps, N.A., 2022. Initial Microstructure Examination of High Burnup Fuel with Varying Operational Burnups. ORNL/SPR-2022/2503.
Snead, M., Yan, Y., Howell, M., Keiser, J., Terrani, K., 2015. Severe Accident Test Station Design Document. ORNL/TM-2015/556.
Sonnenburg, H.W., Wolfgang; Garat, Veronique; Khattout, Farida; Khvostov, Grigory; Raynaud, Partick; Taurines, Tatiana, 2016. Report of Fuel Fragmentation, Relocation and Dispersal. Nuclear Energy Agency.
Turnbull, J.A., Yagnik, S.K., Hirai, M., Staicu, D.M., Walker, C.T., 2015. An Assessment of the Fuel Pulverization Threshold During LOCA-Type Temperature Transients. Taylor & Francis, pp. 477-485.
Yan, Y., Burns, Z., Linton, K., Terrani, K., 2017. Results from In-cell Integral LOCA Testing at ORNL, Water Reactor Fuel Performance Meeting, Jeju Island, Korea.